High Verdet Constant Glass for Magnetic Field Sensors

Xudong Zhao, Weiwei Li, Qi Xia, Ping Lu, Haizheng Tao, Mengling Xia, Xianghua Zhang, Xiujian Zhao, Yinsheng Xu

High Verdet Constant Glass for Magnetic Field Sensor

*Xudong Zhao, Weiwei Li, Qi Xia, Ping Lu, Haizheng Tao, Mengling Xia, Xianghua Zhang, Xiujian Zhao, and Yinsheng Xu**

XD. Zhao, P. Lu, H. Tao, M. Xia, X. Zhang, XJ. Zhao, Y. Xu
State Key Laboratory of Silicate Materials for Architectures, Wuhan University of Technology, Wuhan 430070, China
E-mail: xuyinsheng@whut.edu.cn

W. Li
State Key Laboratory of Advanced Technology for Materials Synthesis and Processing, Wuhan University of Technology, Wuhan 430074, China

Q. Xia
School of Intelligent Manufacturing and Electronic Engineering, Wenzhou University of Technology, Wenzhou 325035, China

X. Zhang
Institut Des Sciences Chimiques de Rennes UMR 6226, CNRS, Université de Rennes 1, Rennes 35042, France

Keywords: Rare-earth ions, Magneto-optical material, Faraday effect, Glass, Magnetic field sensing.

Abstract

Due to the high transparency, high Verdet constant, as well as easy processing property, rare earth ions doped glasses have been demonstrated great potential in magneto-optical

(MO) applications. However, the variation in the valence state of rare earth ions (Tb^{3+} to Tb^{4+}) resulted in the decreased effective concentration of the paramagnetic ions and thus degraded MO performance. Here a strategy was raised to inhibit the oxidation of Tb^{3+} into Tb^{4+} as well as improve the thermal stability by tuning the optical basicity of glass network. Moreover, the depolymerization of the glass network was modulated to accommodate more Tb ions. Thus, a record high effective concentration ($14.19\times10^{21}/cm^3$) of Tb ions in glass was achieved, generating a high Verdet constant of 113 rad/(T·m) at 650 nm. At last, the first application of MO glass for magnetic field sensor was demonstrated, achieving a sensitivity of 0.139 rad/T. We hope our work provides guidance for the fabrication of MO glass with high performance and thermal stability and could push MO glass one step further for magnetic sensing application.

1 Introduction

Magneto-optical (MO) material is significant for application in modern optics, such as fiber sensors, optical isolators, and modulators[1-6], due to the ability of magneto-optic interacting or transforming. As a magneto-optic matrix, MO materials rotate the polarization plane of an incident light beam with the angle as a function of the polarization of the two components of the circularly polarized light, which is usually called the Faraday effect[7]. The MO devices require materials combining high transparency and high Faraday-rotation-angle-dependent Verdet constant as well as easy processing property, ensuring the sufficient transmittance and rotation of the incident light in different application circumstances.

Rare earth ions (Tb^{3+}, Dy^{3+} [8-11], Ho^{3+} [11-13], Er^{3+} [14-16]) are typical paramagnetic ions

for their high magnetic moment, yielding high Verdet constant. Common MO materials, including single crystal (such as $Tb_3Ga_5O_{12}$), transparent ceramic (such as $Tb_3Sc_2Al_3O_{12}$), and thin film doped with rare earth ions (such as $Tb_3Fe_5O_{12}$), can achieve high transmittance and Verdet constant[17-21]. For example, the commercial MO crystal, $Tb_3Ga_5O_{12}$, has a transmittance of over 80% and a high Verdet constant of 121 rad/(T·m) at 650 nm, making it one of the key materials in optical isolator at present. However, these materials are difficult to be further processed, especially limited over long-distance light transmittance and rotation. Glass can be easily processed into any shape and size, and glass fiber manufacturing is a mature technology, making the rare earth doped MO fiber promising. The MO glass fiber has realized a low optical loss of 6.4 dB/m at 880 nm[22]. Furthermore, the tunable composition makes the glass network more inclusive of paramagnetic ions. For example, Tb doping content in GeO_2-PbO-B_2O_3–SiO_2 MO glass reaches a high content of 40 mol% and increases to 45 mol% in GeO_2-B_2O_3-P_2O_5-ZnO MO glass[23, 24]. Besides, owing to the uniform and stable amorphous network structure, MO glass tends to reach higher transmittance at 1064 nm which is attractive for applications in communication and laser systems. Moreover, the mature and rapid automatic machinery in the glass industry makes MO glass compose shorter preparation time, lower cost, and flexible size regulation including either super large size or micro nano size which enable it a promising material in MO devices.

The main challenge of MO glass is the variation in the valence state of rare earth ions, resulting in the decrease of the effective concentration of the paramagnetic ions and thus degraded MO performance. The valence state was dependent on the ability of

glass network structure to gain and lose electrons, also called optical basicity. Additionally, as glass network modifier, high content of rare earth ions may lead to depolymerization of the network, decreasing the thermal stability of glass, which is not conducive to subsequent processing or fiber manufacturing. Nevertheless, a deep understanding of MO performance and the stability associated with glass network has not been reported up to now.

In this work, we choose terbium as the paramagnetic ions and borogermanate glass as the glass matrix and discuss the structure, valance and application of MO glasses. The glass network was tuned by replacing B_2O_3 with Al_2O_3 and maintaining the diamagnetism of the glass matrix for reasonable comparison. Proper increasing Al content increased the network connectivity, inhibiting the oxidation of Tb^{3+} into Tb^{4+} as well as improving the thermal stability. Furthermore, the doping concentration of Tb_2O_3 was increased to 45 mol% while ensuring the transparency of the glass. High effective content of Tb^{3+} resulted in a high Verdet constant of 113 rad/(T·m) at 650 nm. Finally, we assembled our MO glass into a magnetic field sensor, and the sensitivity of the magnetic field measurement reached 0.139 rad/T. This work provides reference for the preparation of MO glass with high effective content of paramagnetic ions.

2 Results and discussion

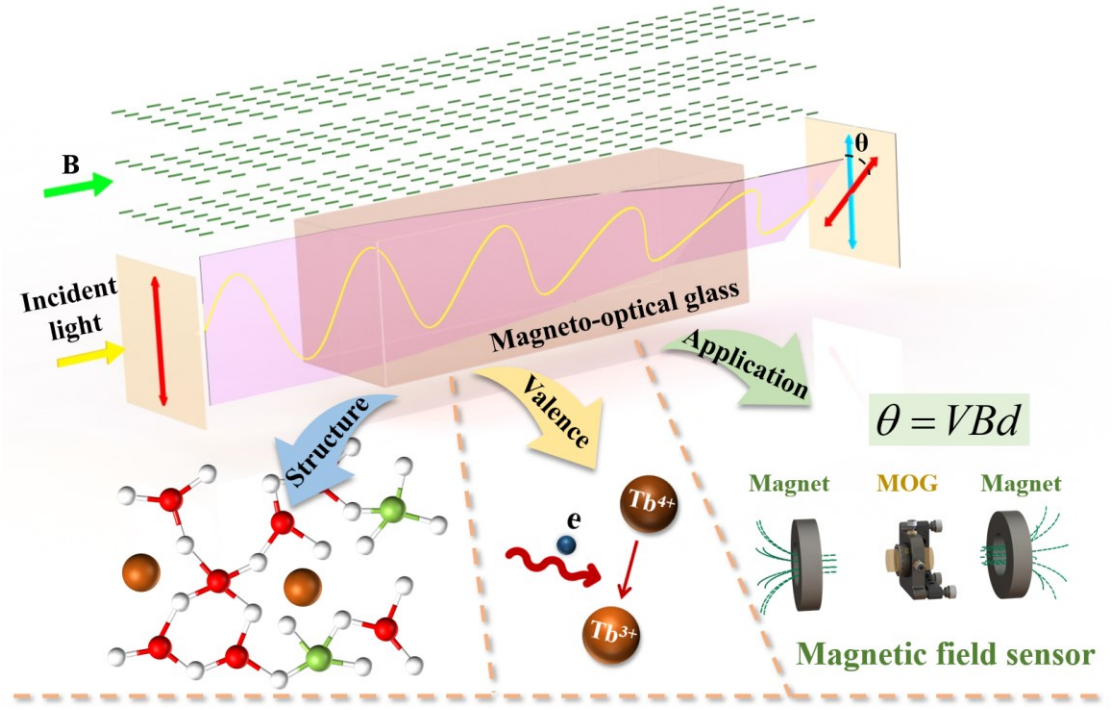

Figure 1 Schematic of Faraday effect and the corresponding key factors associated with MO glass

As illustrated in **Figure 1**, the incident light beam transmitted accompanying with rotating the polarization plane through the MO glass inside a magnetic field (Faraday effect). The rotating angle θ can be obtained according to $\theta=VBd$, where V is Verdet constant, B is magnetic flux density, and d is the thickness of the MO glass. To reduce the workspace and improve the flexibility of the system, high V of the materials is necessary for diminished magnetic field. The effective concentration of paramagnetic ions involved in the MO glass is the prerequisite to achieve a high Verdet constant. Thanks to the amorphous nature of the glass network, i) the depolymerization of the glass network can be controlled to accommodate more rare earth ions, ii) the ratio of different chemical groups that build glass network framework such as [AlO_4], [BO_4]

and [BO_3] can be tuned to adjust the ability of gaining and losing electrons (optical basicity) and thus inhibiting the change of the valence state of rare earth ions.

2.1 Structural analysis

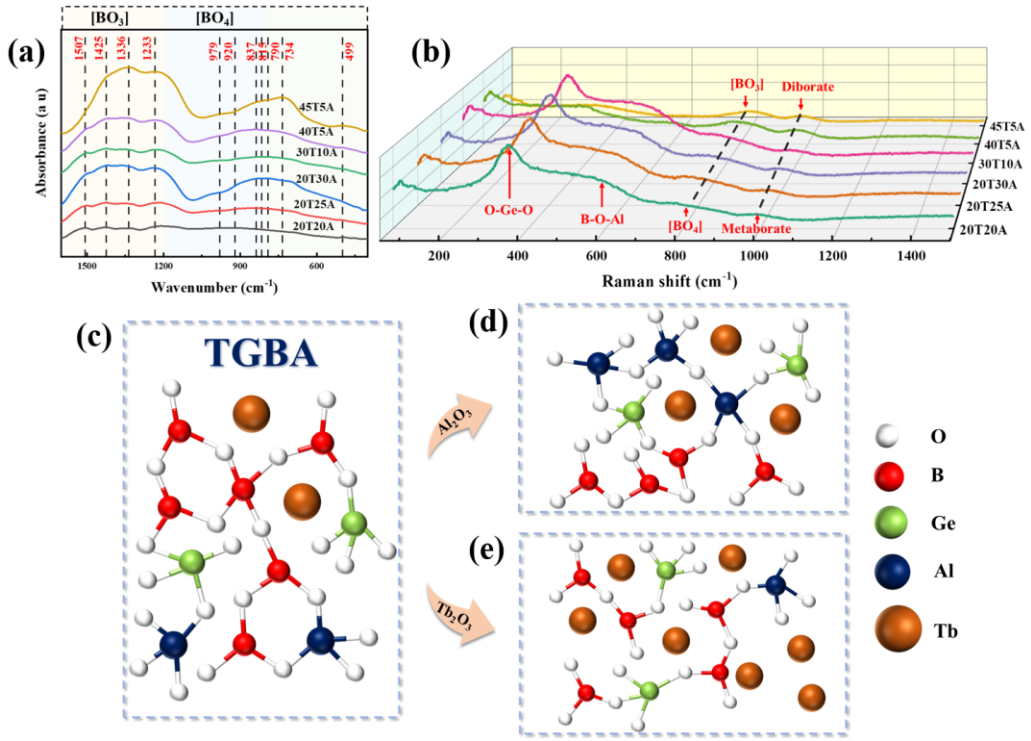

Figure 2 (a) FTIR and (b) Raman spectra of TGBA MO glasses, (c) illustration of the local glass structure with the increase of (d) Al_2O_3 and (e) Tb_2O_3

Firstly, we prepared terbium doped borogermanate glasses (Tb_2O_3-GeO_2-B_2O_3-Al_2O_3) through melt-quenching method. The raw material powders were mixed and heated into high-temperature melt. During the melting process, B_2O_3 and GeO_2, the typical glass “network former”, broke bonds to form B-O and Ge-O randomly crossed network structure, forming a shortrange ordered but long-range disordered amorphous structure. Other ions are connected to the network through bridge-oxygen. Then the

melt was quickly quenched and molded into bulk transparent glass (**Figure S1**) maintaining the network structure. The glass network structure can be tuned by varying the composition. Both aluminum and boron preferentially tend to form tetrahedron combining with O in glasses[25]. Replacing B_2O_3 by Al_2O_3 would not change the network structure of glass significantly, but may effectively change the optical basicity of glass due to the the difference in electronegativity of aluminum and boron.

To verify our assumption, B_2O_3 was partially replaced by Al_2O_3 in MO glasses that contain 20 mol% terbium, and the variation of the network structure was analyzed by infrared spectra and Raman spectra. As shown in **Figure 2a**, there are multiple infrared vibration bands over a wide range of wavenumbers, namely, B-O vibration of $[BO_3]$ triangle unit (1200-1600 cm^{-1}), B-O vibration of $[BO_4]$ tetrahedral units (950-1200 cm^{-1}), B-O vibration of $[BO_4]$ overlap with Al-O vibrations of $[AlO_4]$ units (800-950 cm^{-1}), and Al-O vibrations of $[AlO_4]$ overlap with Ge-O vibrations of $[GeO_4]$ units (500-800 cm^{-1}). [24]. The detailed assignments of the vibration peaks were listed in **Table S2**. With the increased replacement of B_2O_3 by Al_2O_3, $[AlO_4]$ asymmetric stretching vibration at 734 cm^{-1} enhanced obviously while the $[BO_4]$ vibration weakened, indicating Al atoms entered into the structure by replacing B atoms. Taking into account that the enhanced B-O vibration of $[BO_3]$ triangle units, we can conclude that with Al_2O_3 replacing B_2O_3, the $[AlO_4]$ units in the network structure increase and the oxygen atoms of $[BO_4]$ are plundered, resulting in a sharp reduction of $[BO_4]$ and partial conversion to $[BO_3]$ units. Noted that the $[AlO_4]$ units help to increase the network connectivity, thus improving the thermal stability of the MO glass[26, 27].

Then we further increase the terbium content in MO glass and investigate the network structure. With the increased terbium concentration from 20 mol% to 30 mol%, 40 mol% and 45 mol% in the raw materials, the vibration peak of [BO_4] reduces and the [BO_3] peak increases, indicating that part of [BO_4] transformed into [BO_3]. For comparison, the local spectra have been given in the supporting information. As shown in the FTIR absorption spectra (**Figure S2a**), it could be found that a sharp decrease occurs in the range of 950-1200 cm^{-1}, indicating the [BO_4] absorbance decreases with the increase of Al_2O_3. Similarly, the [BO_4] absorbance decreases with the increase of Tb_2O_3 as shown in **Figure S2b**. However, if terbium concentration was further increased to 50 mol%, the composition cannot form glass. This is because terbium is a kind of network modifier that break the glass network greatly, excess terbium may decrease the network connectivity and resulting in the agglomeration of Tb ions[28].

To further confirm the results obtained by FTIR, **Figure 2b** gives the Raman spectra of the MO glasses. The Raman shift of the peaks and their possible assignments have been summarized in **Table S3**. It could be found that GeO_2 is an important network former. With the increase of Tb_2O_3, the peak of O-Ge-O decreases sharply, which indicates the former glass network is broken and Tb_2O_3 acts as network modifier that reduces the network connectivity greatly. Notably, the peak of [BO_4] located at 832 cm^{-1} shifts to [BO_3] located at 806 cm^{-1} can be observed in **Figure 2b** which consists with the results in FTIR spectra. Meanwhile, with the increase of Tb_2O_3, metaborate has the tendency to transform to diborate.

Based on the above results, the local glass structure evolution of MO glass with

the increase of Al_2O_3 and Tb_2O_3 has been given in **Figure 2c.** It could be confirmed that with more Al_2O_3 replacing B_2O_3, the glass network connectivity is enhanced as more [AlO_4] participate in the glass network which results in the decrease of [BO_4] and the increase of bridging oxygen, as shown in **Figure 2d**. Meanwhile, as given in **Figure 2e**, with the increase of Tb_2O_3, the original glass network was interrupted, especially the borate rings, as metaborate depolymerization into diborate, which is corresponding to the peak intensity of [BO_3] strengthening in the FTIR spectra.

2.2 Valance state of Tb and Ge in MO glass

The influence mechanism of glass network structure on the valance state of Tb, which is the key of the effective concentration of paramagnetic ions and the consequent MO property, was clarified by XPS (**Figure S3**). Usually, only Tb^{3+} shows a notable MO response[25, 29]. However, as a raw material, the +3 and +4 valence states of Tb co-exist in the Tb_4O_7. After high temperature melting, two valence state are still co-existed.

Meanwhile, Ge ions may behave as zero valent, divalent or tetravalent ions in the glass which will greatly influence the Tb ions state[30]. Therefore, the valence state in MO glass is mainly discussed.

2.2.1 Valence state of Tb and Ge

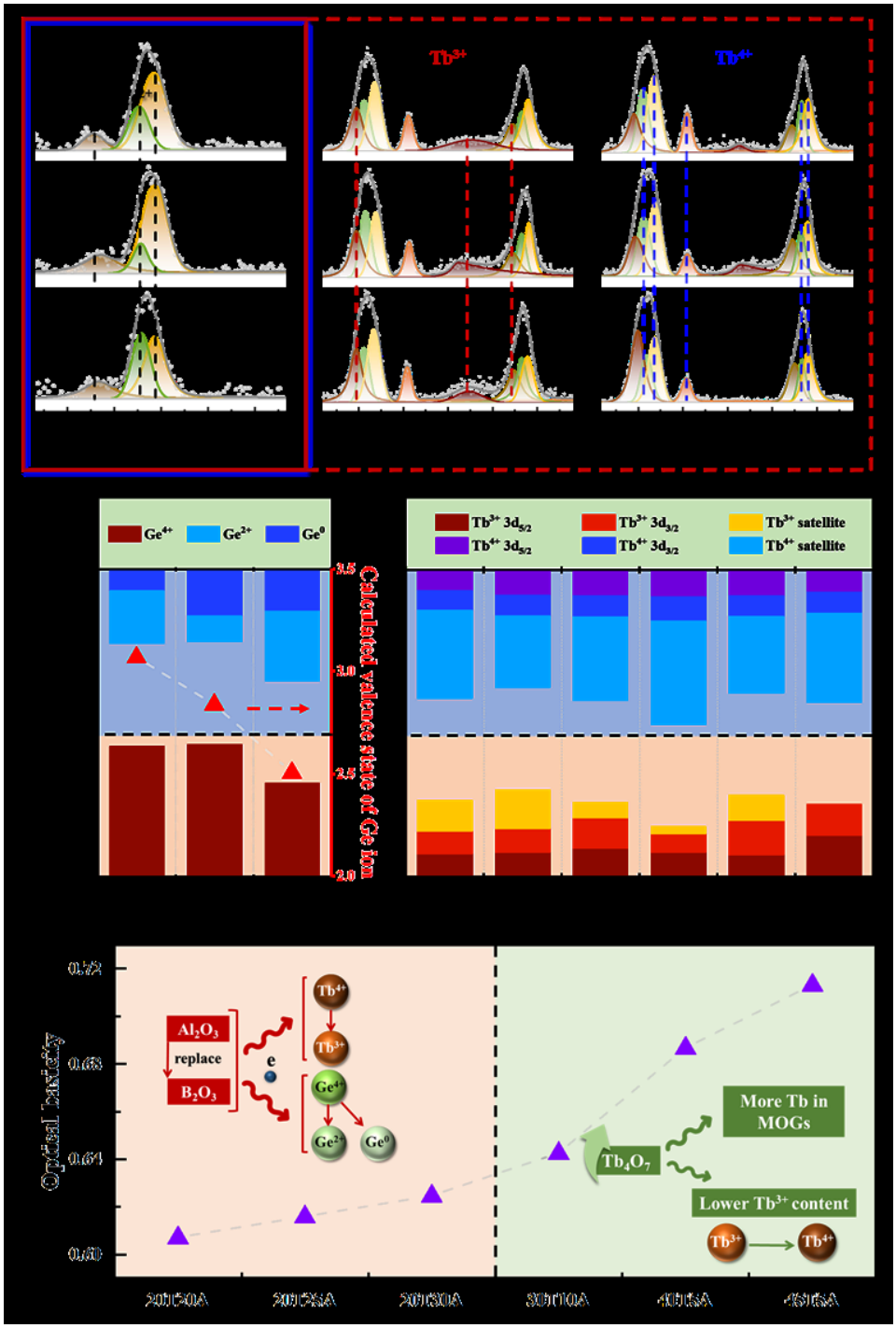

Figure 3 XPS spectra of (a) Ge 3d in MO glasses containing 20 mol% Tb_2O_3 and (b) Tb 3d in MO glasses, (c) Quantitative analysis of Ge ions with different valence states and its calculated valence state, (d) Quantitative analysis of Tb^{3+} and Tb^{4+} among Tb ions, (e) Optical basicity and the electron transfer mechanism in MO glasses with the increase of Al_2O_3 and Tb_4O_7

Figure 3a gives the Ge 3d XPS spectra of 20T20A, 20T25A and 20T30A. Three peaks with binding energy at ~29 eV, ~31.6 eV and ~32.5 eV were observed in Ge 3d spectra, corresponding to Ge^{0}, Ge^{2+} and Ge^{4+}, respectively[30, 31]. The calculated valence states of Ge ions are 3.07, 2.84 and 2.51 in 20T20A, 20T25A and 20T30A, respectively. Through the quantitative analysis of these peaks, Ge ions have the tendency to change from high valence state to low valence state with the increase of Al_2O_3 as shown in **Figure 3c**.

The valence state of Tb ions can also be analyzed by detecting the electron arrangement on 4d or 3d electron orbit. Since the binding energy bands of Tb^{3+} and Tb^{4+} are relatively close and difficult to distinguish in the 4d orbital spectra, the 3d orbital was usually chose for analysis. The Tb 3d XPS spectra of Tb doped glasses are shown in **Figure 3b**. According to the literature[25, 29, 32, 33], peaks in Tb 3d spectra could be divided into two parts. As marked in **Figure 3b**, binding energy at ~1239 eV, ~1263 eV and ~1274 eV corresponding to the Tb^{3+} part, while binding energy at ~1241 eV, ~1243 eV, ~1251 eV, ~1276 eV and ~1278 eV corresponding to the Tb^{4+} ions[32, 33]. The XPS peak positions and their corresponding Tb ion valence were summarized in **Table S4**.

Figure 3d gives the area fraction of the peaks to the spectra. It could be found that when Al_2O_3 replaces B_2O_3, part of Tb^{4+} is transformed into Tb^{3+}, and then into Tb^{4+}. The abnormal valence change of Tb ion indicates the complex electron transfer. Besides, comparing lower Tb doped glasses with higher Tb doped glasses in **Figure 3d**, the area

fractions of Tb^{3+} in 20% Tb_2O_3 doped glasses are greater than the higher Tb_2O_3 doped glasses.

2.2.2 Electron transfer mechanism in MO glass

To understand the electron transfer mechanism in MO glass, the optical basicity was calculated and discussed combining with network structure. The optical basis theory constructs the numerical expression of the average electron transfer capacity of different oxides to predict the valence state of multivalent ions in glass. According the **Formula (2)** in supporting information, **Figure 3e** gives the calculated optical basicity of MO glasses. It could be found that the optical basicity increases with the increase of Al_2O_3 or Tb_2O_3.

As the content of Al_2O_3 increases from 20 mol% to 25 mol%, Λ_{th} increases, more electrons enter the glass network. According to the Tb 3d and Ge 3d spectra, the process of $Tb^{4+} \rightarrow Tb^{3+}$ and $Ge^{2+} \rightarrow Ge^0$ occur simultaneously and are dominated by the former. Hence, 20T25A has a higher Tb^{3+} content than that of 20T20A. While the continuous addition of Al_2O_3 does not result in higher Tb^{3+} content, it turns out that Tb^{3+} content in 20T30A is quite low. As shown in **Figure 3c**, great amount of Ge^{4+} turn into Ge^{2+} or Ge^0, this process inhibits Tb^{4+} obtaining electrons which result in the relatively low Tb^{3+} content. As mentioned above, the increase of Al_2O_3 greatly enhance the network connectivity, and the Tb ions are easily to obtain electrons. While the high connectivity glass network implies the connectivity with Ge ions strengthens as well, which cause the Ge ions getting electrons.

On the other hand, as shown in **Figure 3e**, the optical basicity increases in proportion to Tb_2O_3 content. However, the high optical basicity of Tb_2O_3 makes Tb^{3+} easy to lose electrons and oxidize to Tb^{4+}. That is why the proportion of Tb^{3+} is low when the content of Tb_2O_3 is high. Furthermore, the increase of Tb_2O_3 makes Tb ions agglomerating in the glass network, which results in partial Tb ions no way to contact Ge-B-Al glass network, and this may also lead to high content of Tb^{4+}.

2.3 Optical properties

As a kind of lens material, the optical properties show great importance in the application. Better transmittance indicates the possible application of fiber and large size glass which optical path is long. Besides, the luminescent property of Tb ion is another potential application. Hence, in this section, the optical properties are discussed in detail.

2.3.1 Transmission spectra

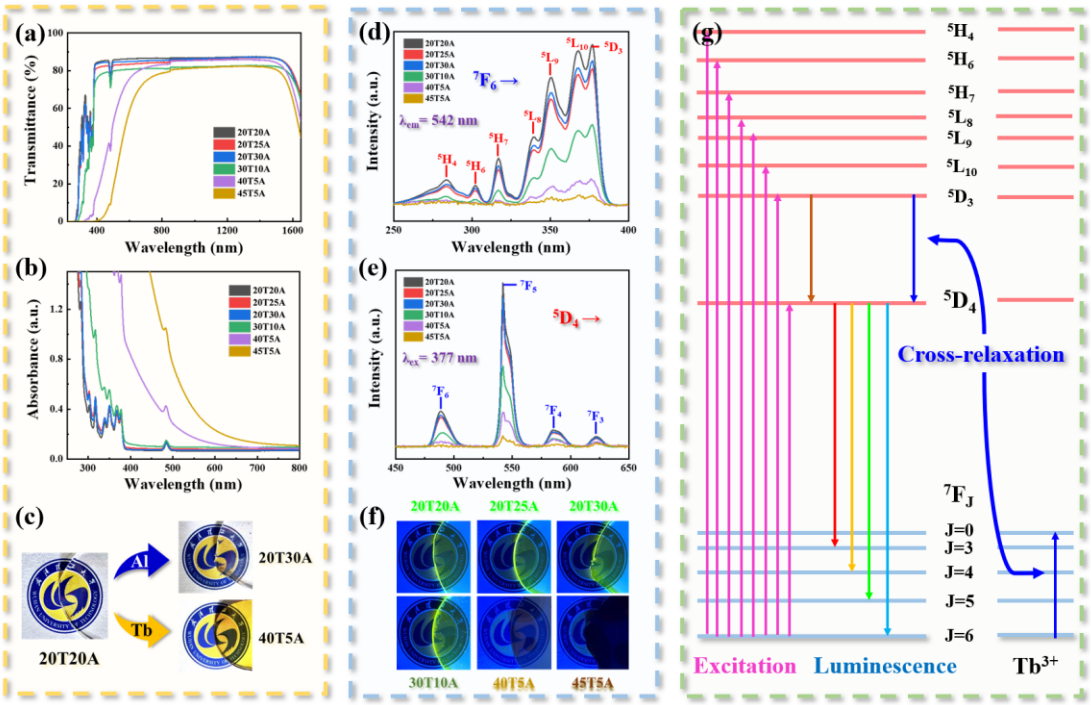

Figure 4 (a) Transmission and (b) absorption spectra of the polished MO glasses, (c) Color change of MO glasses with the increase of Al_2O_3 and Tb_2O_3, (d)Excitation and (e) emission spectra of MO glasses, (f) Luminous picture of the polished MO glasses, (g) Energy transfer process of Tb^{3+} ions

The transmission and absorption spectra of the polished MO glasses are shown in **Figure 4a** and **4b**, respectively. The typical absorption peak at about 483 nm is the $^7F_6 \rightarrow {}^5D_4$ electron transition of Tb^{3+}[34]. The average transmittance of MO glasses containing 20 mol% Tb_2O_3 among 400-1600 nm is above 85%. As shown in **Figure 4c**, with the increase of Al_2O_3, MO glass maintain its transparency. While, with the increase of Tb_2O_3, MO glass starts to get brown and the color gets darken with the further increase of Tb_2O_3 as shown in **Figure S1**. Moreover, as shown in **Figure S4**, the band gap E_g was calculated. With the increase of terbium, E_g decreases due to the high

polarizability of Tb ions. Meanwhile, as glass is uniform and amorphous, the band gap is related to the bonding energy of the glass network. As the upper edge of the valence band is linear in relationship with the gone pairs of p electrons on the oxygen-bridging atoms, the band gap increases with increasing bonding energy. With the increase of Tb ions, the bridge oxygen in the network structure decreases, considering the bond between rare earth ions and oxygen ions is weaker than that between the network formation ions (Ge, B, and Al) and oxygen ions, the glass network connectivity and band gap decrease, resulting in the absorption edge in the UV region gradually move towards the direction of long wavelength.

2.3.2 Luminescent properties

The excitation spectrum of TGBA is shown in **Figure 4d**. It can be found that the excitation band of TGBA glass from 250 to 400 nm is mainly located at 284 nm, 301 nm, 316 nm, 339 nm, 350 nm, 369 nm and 377 nm corresponding to the transitions of $^7F_6 \rightarrow {}^5H_4$, $^7F_6 \rightarrow {}^5H_6$, $^7F_6 \rightarrow {}^5H_7$, $^7F_6 \rightarrow {}^5L_8$, $^7F_6 \rightarrow {}^5L_9$, $^7F_6 \rightarrow {}^5L_{10}$ and $^7F_6 \rightarrow {}^5D_3$ of Tb^{3+} ions[35]. It turns out that the position of excitation band basically unchanged, as the 4f electron of Tb^{3+} ion is shielded by $5s^25p^6$ shell[36]. With the increase of Tb_2O_3, the intensity of excitation band decreases gradually.

Figure 4e gives the emission (PL) spectra of TGBA MO glasses at the excitation wavelength of 377 nm where the excitation intensity is the greatest. The luminescence of MO glass mainly comes from Tb^{3+} with $^5D_4 \rightarrow {}^7F_J$ energy level transition: $^5D_4 \rightarrow {}^7F_6$ (489 nm), $^5D_4 \rightarrow {}^7F_5$ (544 nm), $^5D_4 \rightarrow {}^7F_4$ (585 nm) and $^5D_4 \rightarrow {}^7F_3$ (621 nm). Since

the $^5D_4 \rightarrow {}^7F_5$ transition probability of Tb^{3+} ion is the largest under the excitation of 377 nm, the yellow-green fluorescence is the strongest at 544 nm. **Figure 4f** gives the luminous picture of the polished TGBA MO glasses. In addition, with the increase of Tb^{3+} ion, the ion spacing decreases, and the luminous intensity of MO glasses decreases gradually. To clarify this, we calculated the critical distance R_c between Tb^{3+} ions as shown in **Figure S5**, it could be found that with the increase of Tb^{3+} ion doping concentration, the critical distance decreases from 0.65 to 0.52 nm. As rare earth ions exceed the luminescence quenching concentration, the center distance is smaller than the critical value, the energy transfer probability increases and the cross-relaxation of $^5D_3 + {}^7F_6 \rightarrow {}^5D_4 + {}^7F_0$ occurs, which greatly weakens the luminescence intensity. In particular, the luminescence intensity of 40T5A and 45T5A is very weak, which is mainly due to the agglomeration of Tb^{3+}, and energy is continuously transferred to the next activation centre until it reaches the quenching center, and then concentration quenching occurs, which weakens the luminescence intensity of the glass. In order to describe the energy transfer process of Tb^{3+} ions more clearly, the energy level transitions of Tb^{3+} ions have been plotted in **Figure 4g**.

2.4 Magneto-optical property

As the most important property of MO glass, the MO property determines the Faraday effect. To verify the relationship between valence states and MO property, the proportion of Tb^{3+} in MO glass is calculated. Besides, the MO glass is assembled for magnetic field sensing after evaluating its Verdet constant.

2.4.1 Tb^{3+} concentration in MO glass

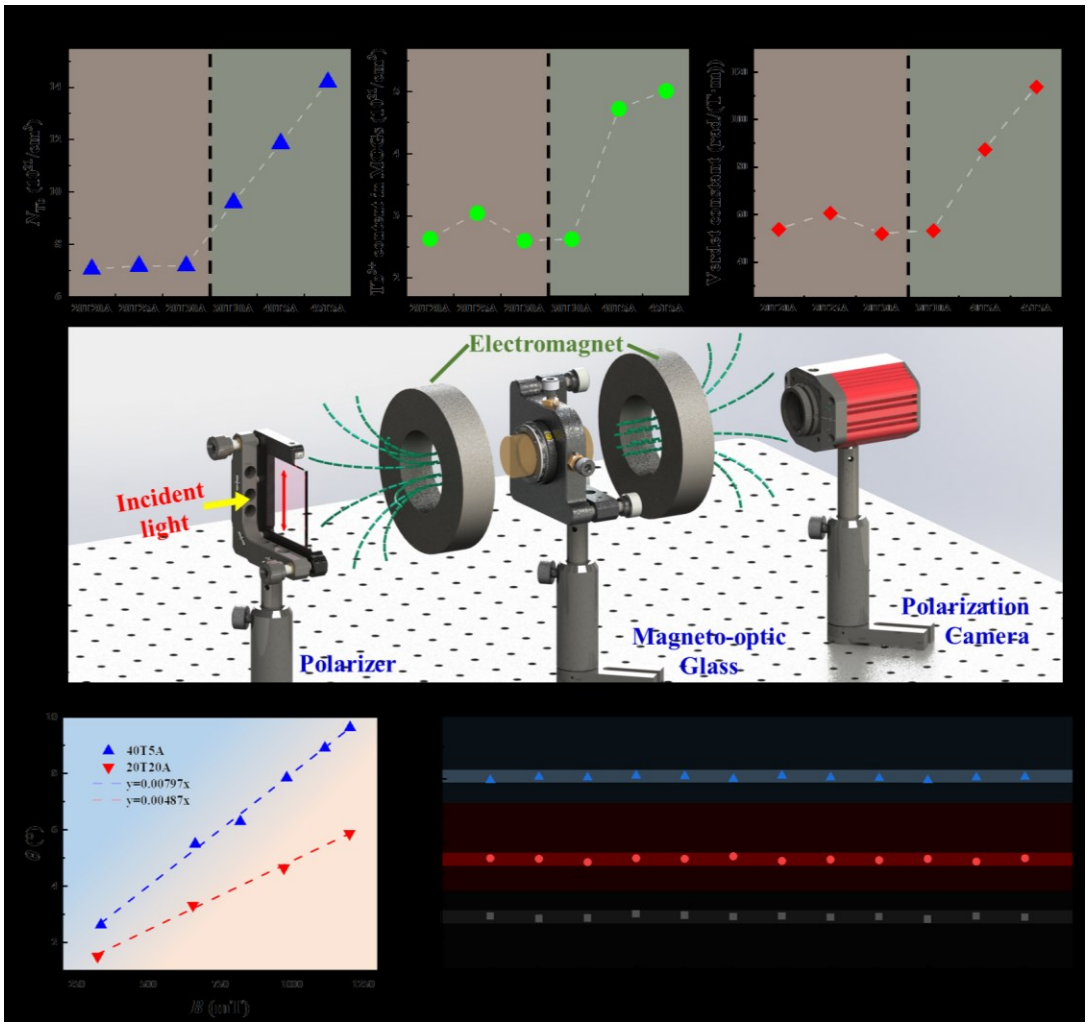

Figure 5 (a)Effective concentration of Tb ions, (b) Content of Tb^{3+} in MO glasses, (c) Verdet constant of MO glasses at 650 nm, (d) schematic of magnetic field sensing, (e) relationship between the rotation angle and magnetic field intensity of 20T20A and 40T5A, (f) sensing stability of MO glass with the extension of test time.

The effective concentration of Tb ions, N_{Tb}, a parameter that represents the proportion of Tb ions successfully entering the glass network[28, 37]. As the paramagnetism of MO glass origin from Tb^{3+}, N_{Tb} is helpful to predict the MO

performance of glass. Simulated with the **Formula (3)** in supporting information, as shown in **Figure 5a**, the N_{Tb} will significantly increase with the increase of Tb_2O_3, whereas the increase of Al_2O_3 almost has no effect on N_{Tb}. Furthermore, considering the proportion of Tb^{3+} among Tb ions, the concentration of Tb^{3+} in MO glass ($C_{Tb}{}^{3+}$) is then calculated with **Formula (4)** in supporting information. As given in **Figure 5b** and **5c**, the total amount of Tb^{3+} in MO glasses shows the same tendency with the Verdet constant, which indicates the amount of Tb^{3+} dominate the MO property of MO glass.

2.4.2 Verdet constant and application for magnetic field sensor

The main criterion for evaluating the MO properties of MO glass is Verdet constant, which is directly proportional to the concentration of paramagnetic ions. As shown in **Figure 5c**, the Verdet constants of MO glasses were tested at 650 nm under room temperature. Overall, the Verdet constants of these MO glasses show the same trends with $C_{Tb}{}^{3+}$. Since Tb^{3+} is paramagnetic and Tb^{4+} is diamagnetic, largest Tb^{3+} content in 20T25A results in its greatest Verdet constant when there is 20% Tb_2O_3 in MO glasses.

Moreover, with the increase of Tb_2O_3, the Verdet constant of MO glass shows an increasing tendency. Among them, V_{30T10A} is low, which is mainly due to the low content of Tb^{3+} as shown in **Figure 5b**. After testing the MO properties of commercial TGG ceramics by the same equipment, V_{TGG} turns out to be 121 rad/(T·m) at 650 nm which is consist with the literature[38]. Meanwhile, V_{45T5A} in this work is 113 rad/(T·m), which shows that MO glass has great potential to replace TGG ceramics after further composition regulation. Since the proportion between Al_2O_3 and B_2O_3, the content of

GeO_2 can greatly affect the structure of glass network and the ionic valence, to further increase the Verdet constant of 45T5A, reducing GeO_2 or increasing Al_2O_3 is a good choice.

As a kind of Faraday material, magnetic field sensing is an important application for MO glass. **Figure 5d** gives the testing platform for magnetic field sensing based on 20T20A and 40T5A MO glasses. **Figure 5e** gives the sensing data and fitting curve of MO glasses. It could be found that the rotation angle (θ) changes in proportion to the magnetic flux density (B). As 40T5A has greater Verdet constant, its sensing sensitivity is better. From the corresponding fitting curve, the sensitivity of the 40T5A magnetic field measurement reached 0.139 rad/T. And the coefficient of determination (R-square) due to error of such measurement was 0.997. Moreover, the sensor stability with its running time of 40T5A is tested as well. As shown in **Figure 5f**, the magnetic sensor has excellent sensing stability at low or high magnetic flux density in an hour which enables it for long time use.

3 Conclusion

A series of Tb-doped GeO_2-B_2O_3-Al_2O_3 glasses were prepared via melt-quenching, and the structure and valence changing mechanism were discussed in detail. After optimizing the calculation formula of the effective concentration of Tb ions (N_{Tb}), we calculated the concentration of Tb^{3+} in MO glass ($C_{Tb}{}^{3+}$) and found that the MO property was highly consistent with the content of trivalent terbium ions in the glass. The MO glass reaches the highest Verdet constant of 113 rad/(T·m) at 650 nm as the

content of Tb_2O_3 was 45 mol%. Meanwhile, the first application of MO glass for magnetic field sensor was realized, achieving a sensitivity of 0.139 rad/T and good working stability. To further increase its Verdet constant, increasing Al_2O_3 is a feasible option, as Al_2O_3 could enhance the glass network connectivity and make more tetravalent terbium into trivalent. A record high effective concentration ($14.19\times10^{21}/cm^3$) of Tb ions in glass was achieved.

Supporting Information

The Supporting Information is available free of charge at

Magneto-optical (MO) glass preparation; Table S1 Composition of glass studied; Figure S1 Pictures of the transparent MO glasses; Characterization; Table S2 FTIR spectral assignments; Figure S2 FTIR absorption spectra of [BO_4] tetrahedral units in the range of 950-1200 cm^{-1} with the increase of (a) Al_2O_3 and (b) Tb_2O_3; Table S3 Raman spectral assignments; Figure S3 XPS full spectrum of 20T20A sample; Table S4 XPS peak positions and their corresponding assignments; Table S5 XPS peak positions and their corresponding Ge ion valence; Calculation of band gap; Figure S4 Band gap of these MO glasses; Calculation of critical distance between Tb^{3+} ions; Figure S5 Critical distance R_c between Tb^{3+} ions; Figure S6 The density of these MO glasses; Calculation of optical basicity; Figure S7 Thermal properties ($\Delta T = T_x - T_g$) of MO glasses; Calculation of Tb^{3+} content in MO glasses; Table S6 Summarization of the experimental data.

Acknowledgement

This work is financially supported by the National Natural Science Foundation of China (U2241236, 61975156, 61905082), State Key Laboratory of Silicate Materials for Architectures (Wuhan University of Technology, SYSJJ2021-01)

References

(1) Higo, T.; Man, H. Y.; Gopman, D. B.; Wu, L.; Koretsune, T.; van't Erve, O. M. J.; Kabanov, Y. P.; Rees, D.; Li, Y. F.; Suzuki, M. T.; Patankar, S.; Ikhlas, M.; Chien, C. L.; Arita, R.; Shull, R. D.; Orenstein, J. and Nakatsuji, S. Large Magneto-optical Kerr Effect and Imaging of Magnetic Octupole Domains in An Antiferromagnetic Metal. *Nat. Photonics* **2018**, 12, 73.

(2) Truppe, S.; Williams, H. J.; Hambach, M.; Caldwell, L.; Fitch, N. J.; Hinds, E. A.; Sauer, B. E. and Tarbutt, M. R. Molecules Cooled Below the Doppler Limit. *Nat. Phys.* **2017**, 13, 1173.

(3) Chin, J. Y.; Steinle, T.; Wehlus, T.; Dregely, D.; Weiss, T.; Belotelov, V. I.; Stritzker, B. and Giessen, H. Nonreciprocal Plasmonics Enables Giant Enhancement of Thin-film Faraday Rotation. *Nat. Commun.* **2013**, 4, 1599.

(4) Barry, J. F.; McCarron, D. J.; Norrgard, E. B.; Steinecker, M. H. and DeMille, D. Magneto-optical Trapping of A Diatomic Molecule. *Nature* **2014**, 512, 286.

(5) Armelles, G.; Cebollada, A.; García-Martín, A. and González, M. U. Magnetoplasmonics: Combining Magnetic and Plasmonic Functionalities. *Adv. Opt. Mater.* **2013**, 1, 10-35.

(6) Schmidt, M. A.; Wondraczek, L.; Lee, H. W.; Granzow, N.; Da, N. and Russell, P. S. J. Complex Faraday Rotation in Microstructured Magneto-optical Fiber Waveguides. *Adv. Mater.* **2011**, 23, 2681-2688.

(7) Wu, L.; Salehi, M.; Koirala, N.; Moon, J.; Oh, S. and Armitage, N. P. Quantized Faraday and Kerr Rotation and Axion Electrodynamics of A 3D Topological Insulator. *Science* **2016**, 354, 1124-1127.

(8) Dinca, M. C.; Sava, B. A.; Galca, A. C.; Kuncser, V.; Iacob, N.; Stan, G. E.; Boroica, L.; Filip, A. V. and Elisa, M. Magneto-optical Properties of Borophosphate Glasses Co-doped with Tb^{3+} and Dy^{3+} Ions. *J Non-Cryst. Solids* **2021**, 568, 120967.

(9) Guo, H.; Song, J.; Gong, Y.; Yin, H.; Mo, Z.; Yatongchai, C.; Li, Y. and Buchanan, R. C. The Crystallization Behavior of Dy^{3+}/Tb^{3+} Doped Aluminoborosilicate Glasses. *J Non-Cryst. Solids* **2017**, 470, 189-193.

(10) Pisarski, W. A.; Pisarska, J.; Żur, L. and Goryczka, T. Structural and Optical Aspects for Eu^{3+} and Dy^{3+} Ions in Heavy Metal Glasses Based on $PbO–Ga_2O_3–XO_2$ (X=Te, Ge, Si). *Opt. Mater.* **2013**, 35, 1051-1056.

(11) Lu, B.; Wu, S.; Cheng, H.; Ye, R.; Cai, X.; Wang, M. and Wang, Y. Binary Transparent $(Ho_{1-x}Dy_x)_2O_3$ Ceramics: Compositional Influences on Particle Properties, Sintering Kinetics and Faraday Magneto-optical Effects. *J. Eur. Ceram. Soc.* **2021**, 41, 2826-2833.

(12) Chen, Z.; Yang, L.; Wang, X. and Yin, H. High Magneto-optical Characteristics of Holmium-doped Terbium Gallium Garnet Crystal. *Opt. Lett.* **2016**, 41, 2580-2583.

(13) Cheng, H.; Lu, B.; Liu, Y.; Zhao, Y.; Sakka, Y. and Li, J.-G. Transparent Magneto-Optical Ho_2O_3 Ceramics: Role of Self-reactive Resultant Oxyfluoride Additive and Investigation of Vacuum Sintering Kinetics. *Ceram. Int.* **2019**, 45, 14761-14767.

(14) Khartsev, S. I. and Grishin, A. M. High Performance Latching-type Luminescent Magneto-optical Photonic Crystals. *Opt. Lett.* **2011**, 36, 2806-2808.

(15) Guo, Q.; Wen, J.; Huang, Y.; Wang, W.; Pang, F.; Chen, Z.; Luo, Y.; Peng, G.-D. and Wang, T. Magneto-optical Properties and Measurement of the Novel Doping Silica Optical Fibers. *Measurement* **2018**, 127, 63-67.

(16) McClelland, J. and Hanssen, J. Laser Cooling without Repumping: A Magneto-Optical Trap for Erbium Atoms. *Phys. Rev. Lett.* **2006**, 96, 143005.

(17) Yin, T.; Ulman, K. A.; Liu, S.; Granados del Águila, A.; Huang, Y.; Zhang, L.; Serra, M.; Sedmidubsky, D.; Sofer, Z.; Quek, S. Y. and Xiong, Q. Chiral Phonons and Giant Magneto-optical Effect in $CrBr_3$ 2D Magnet. *Adv. Mater.* **2021**, 33, 2101618.

(18) Perkinson, C. F.; Einzinger, M.; Finley, J.; Bawendi, M. G. and Baldo, M. A. Magnetic-field-switchable Laser via Optical Pumping of Rubrene. *Adv. Mater.* **2022**,

34, 2103870.

(19) Kustov, M.; Grechishkin, R.; Gusev, M.; Gasanov, O. and McCord, J. A Novel Scheme of Thermographic Microimaging Using Pyro-magneto-optical Indicator Films. *Adv. Mater.* **2015**, 27, 5017-5022.

(20) Wu, Y.; Sun, Z.; Feng, G.; Wang, S.; Xu, L. and Wu, S. Preparation and Properties of Novel $Tb_3Sc_2Al_3O_{12}$ (TSAG) Magneto-optical Transparent Ceramic. *J. Eur. Ceram. Soc.* **2021**, 41, 195-201.

(21) Fakhrul, T.; Tazlaru, S.; Khurana, B.; Beran, L.; Bauer, J.; Vancik, M.; Marchese, A.; Tsotsos, E.; Kucera, M.; Zhang, Y.; Veis, M. and Ross, C. A. High Figure of Merit Magneto-optical Ce- and Bi-Substituted Terbium Iron Garnet Films Integrated on Si. *Adv. Opt. Mater.* **2021**, 9, 2100512.

(22) Franco, D. F.; Ledemi, Y.; Correr, W.; Morency, S.; Afonso, C. R. M.; Messaddeq, S. H.; Messaddeq, Y. and Nalin, M. Magneto-optical Borogermanate Glasses and Fibers Containing Tb^{3+}. *Sci. Rep.* **2021**, 11, 9906.

(23) Yang, H. and Zhu, Z. Magneto-optical Glass Mixed with Tb^{3+} Ions: High Verdet Constant and Luminescence Properties. *J. Lumin.* **2021**, 231, 117804.

(24) Zhou, L. and Zhu, Z. Magneto-optical and Luminescent Properties of Tb^{3+} Ions Doped GBPZ Magneto-optical Glass. *J. Non-Cryst. Solids* **2021**, 574, 121165.

(25) Zhang, Y.; Murai, S.; Maeno, A.; Kaji, H.; Shimizu, M.; Shimotsuma, Y.; Ma, Z.; Qiu, J. and Tanaka, K. Microstructure and Faraday Effect of Tb_2O_3-Al_2O_3-SiO_2-B_2O_3 Glasses for Fiber-based Magneto-optical Applications. *J. Am. Ceram. Soc.* **2021**, 105, 1198.

(26) Ando, M. F.; Fuhrmann, S.; Pan, Z.; Rodrigues, B. P.; Mori, T.; Ebbinghaus, S. G.; Wondraczek, K.; Kitani, S. and Wondraczek, L. Boson Peak and Structural Heterogeneity in Ternary SiO_2-Al_2O_3-B_2O_3 Glasses. *J. Am. Ceram. Soc.* **2021**, 104, 4991-5000.

(27) Kwinda, T. I.; Koppka, S.; Sander, S. A. H.; Kohns, R. and Enke, D. Effect of Al_2O_3 on Phase Separation and Microstructure of R_2O-B_2O_3-Al_2O_3-SiO_2 Glass System (R = Li, Na). *J. Non-Cryst. Solids* **2020**, 531, 119849.

(28) Yin, H.; Gao, Y.; Gong, Y.; Buchanan, R.; Song, J. and Li, M. Wavelength

Dependence of Tb^{3+} Doped Magneto-optical Glass Verdet Constant. *Ceram. Int.* **2018**, 44, 10929-10933.

(29) Yin, H.; Gao, Y.; Guo, H.; Wang, C. and Yang, C. Effect of B_2O_3 Content and Microstructure on Verdet Constant of Tb_2O_3-Doped GBSG Magneto-optical Glass. *J. Phys. Chem. C* **2018**, 122, 16894-16900.

(30) Zatsepin, A. F.; Zatsepin, D. A.; Zhidkov, I. S.; Kurmaev, E. Z.; Fitting, H. J.; Schmidt, B.; Mikhailovich, A. P. and Lawniczak-Jablonska, K. Formation of Ge^0 and GeO_x Nanoclusters in Ge^+-implanted SiO_2/Si Thin-film Heterostructures under Rapid Thermal Annealing. *Appl. Surf. Sci.* **2015**, 349, 780-784.

(31) Takebe, H.; Maeda, H. and Morinaga, K. Compositional Variation in the Structure of Ge–S Glasses. *J. Non-Cryst. Solids* **2001**, 291, 14-24.

(32) Blanco, G.; Pintado, J. M.; Bernal, S.; Cauqui, M. A.; Corchado, M. P.; Galtayries, A.; Ghijsen, J.; Sporken, R.; Eickhoff, T. and Drube, W. Influence of the Nature of the Noble Metal (Rh,Pt) on the Low-temperature Reducibility of A Ce/Tb Mixed Oxide with Application as TWC Component. *Surf. Interface Anal.* **2002**, 34, 120-124.

(33) Nagpure, I. M.; Pitale, S. S.; Coetsee, E.; Ntwaeaborwa, O. M.; Terblans, J. J. and Swart, H. C. Low Voltage Electron Induced Cathodoluminescence Degradation and Surface Characterization of $Sr_3(PO_4)_2$:Tb Phosphor. *Appl. Surf. Sci.* **2011**, 257, 10147-10155.

(34) Zuo, C.; Huang, J.; Liu, S.; Xiao, A.; Shen, Y.; Zhang, X.; Zhou, Z. and Zhu, L. Luminescence and Energy Transfer of Tb^{3+}–doped BaO–Gd_2O_3–Al_2O_3–B_2O_3–SiO_2 Glasses. *Spectrochim. Acta A Mol. Biomol. Spectrosc.* **2017**, 187, 181-185.

(35) Linganna, K.; Sreedhar, V. B. and Jayasankar, C. K. Luminescence Properties of Tb^{3+} Ions in Zinc Fluorophosphate Glasses for Green Laser Applications. *Mater. Res. Bull.* **2015**, 67, 196-200.

(36) Dharmaiah, P.; Viswanath, C. S. D.; Basavapoornima, C.; Krishnaiah, K. V.; Jayasankar, C. K. and Hong, S.-J. Luminescence and Energy Transfer in Dy^{3+}/Tb^{3+} Co-doped Transparent Oxyfluorosilicate Glass-ceramics for Green Emitting Applications. *Mater. Res. Bull.* **2016**, 83, 507-514.

(37) Ding, J.; Man, P.; Chen, Q.; Guo, L.; Hu, X.; Xiao, Y.; Su, L.; Wu, A.; Zhou, Y. and

Zeng, F. Influence of Tb^{3+} Concentration on the Optical Properties and Verdet Constant of Magneto-optic ABS-PZZ Glass. *Opt. Mater.* **2017**, 69, 202-206.

(38) Slezak, O.; Yasuhara, R.; Lucianetti, A. and Mocek, T. Wavelength Dependence of Magneto-optic Properties of Terbium Gallium Garnet Ceramics. *Opt. Express* **2015**, 23, 13641-13647.